

Observation of the quantized motion of excitons in CdSe nanoplatelets

Michele Failla,¹ Francisco Garca Flórez,² Bastiaan B. V. Salzmann,³
Daniel Vanmaekelbergh,³ Henk T. C. Stoof,² and Laurens D. A. Siebbeles¹

¹*Chemical Engineering Department, Delft University of Technology, Van der Maasweg 9, NL-2629 HZ Delft, The Netherlands*

²*Institute for Theoretical Physics and Center for Extreme Matter and Emergent Phenomena, Utrecht University, Princetonplein 5, 3584 CC Utrecht, The Netherlands*

³*Debye Institute, Condensed Matter and Interfaces, Utrecht University, PO Box 80.000, 3508 TA Utrecht, The Netherlands*

We show that the finite lateral sizes of ultrathin CdSe nanoplatelets strongly affect both their photoluminescence and optical absorption spectra. This is in contrast to the situation in quantum wells, in which the large lateral sizes may be assumed to be infinite. The lateral sizes of the nanoplatelets are varied over a range of a few to tens of nanometers. For these sizes excitons experience in-plane quantum confinement, and their center-of-mass motion becomes quantized. Our direct experimental observation of the discretization of the exciton center-of-mass states can be well understood on the basis of the simple particle-in-a-box model.

Cadmium selenide nanoplatelets (CdSe-NPLs) are solution-processable two-dimensional semiconductor nanomaterials which are grown with an atomically precise thickness [1, 2], see Fig. 1(a) and (b). They receive considerable attention due to promising optical properties for optoelectronic applications, including strong optical oscillator strength [3], large exciton binding energy [3–5], weak exciton-phonon coupling [4], high photoluminescence (PL) quantum yield [6], efficient two-photon absorption [7–9], and lasing [7, 10, 11].

The steady-state optical absorption spectrum exhibits well-resolved peaks due to the formation of heavy-hole (HH) and light-hole (LH) excitons, see Fig. 1(c). The energy at which the HH and LH peaks appear in the optical absorption spectrum, as well as the PL energy, strongly depend on the NPL thickness, L_z in Fig. 1(a), which is of the order of a nanometer [1, 12]. Hence, in a NPL excitons are strongly quantum confined along this (vertical) direction.

Besides the atomically precise thickness, the lateral sizes of CdSe-NPLs, L_x and L_y in Fig. 1(a), can also be tuned from a few to tens of nanometers by varying the synthesis procedure [13]. The strong vertical and weak, intermediate or strong in-plane quantum confinement regimes [14, 15] make the optical properties of NPLs to be in between those of quantum wells (with lateral sizes exceeding microns or larger) and quantum dots. Experimentally, reducing the lateral sizes of CdSe-NPLs has been reported to blue shift and narrow the optical absorption and PL peaks [12, 13, 16], decrease the absorption cross section [17] and affect the optical gain and amplified spontaneous emission [17–21].

An interesting peculiarity, commonly observed in the absorption spectrum of CdSe-NPLs, is the asymmetric shape of the HH exciton peak which exhibits a tail at the side of higher photon energy, see Fig. 1(c), whose explanation has been inconclusive. It has for instance been ascribed to fluctuations in the confining potential of NPLs that lead to localization and consequently an increased energy of the excitons [3, 5, 10, 22], or to internally excited exciton states [23, 24]. As depicted

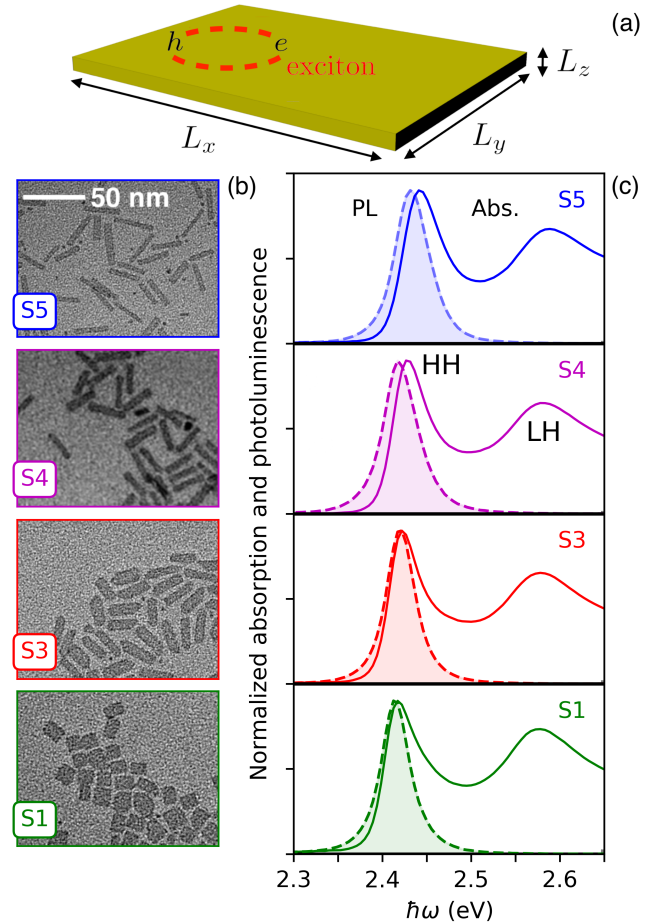


FIG. 1. (a) Scheme of a nanoplatelet. The exciton center-of-mass motion is influenced by the lateral sizes L_x and L_y . (b) TEM images of the investigated CdSe-NPLs. (c) Photoluminescence (dashed lines) and optical absorption (solid) spectra for samples in (b). The absorption peaks at low and high energies are due to HH and LH excitons, respectively.

in Fig. 1(a), excitons have a Bohr radius much smaller than the lateral dimensions of a NPL. Hence, the centre-of-mass (COM) translational motion in the plane of a

Sample	L_x^{avg} (nm)	L_y^{avg} (nm)	Area (nm ²)	r_l
S5	29.3 ± 3.3	5.4 ± 0.8	159	5.4
S4	26.1 ± 3.3	6.4 ± 1.1	167	4.1
S3	25.4 ± 2.9	8.1 ± 0.9	204	3.2
S1	13.7 ± 2.2	13.4 ± 1.9	183	1.0

TABLE I. Average lateral sizes ($L_x^{\text{avg}}, L_y^{\text{avg}}$), area and aspect ratio, r_l , of the CdSe-NPLs samples. Samples are labeled based on their aspect ratio.

NPL must also be considered, and photoexcitation to COM motional states with nonzero in-plane momentum can indeed give rise to the high-energy tail of the HH exciton peak. Until now, however, this COM motion of an exciton has not yet been invoked to explain the PL and absorption spectra. The finite lateral size of NPLs then also affects the COM energy of excitons, as discussed by Richter [15]. The presence of these states has also been invoked to explain the exciton dynamics probed by transient resonant four-wave mixing [3] and transient PL spectra at temperatures below 200 K [25, 26]. The latter exhibits two PL peaks with a lateral size-dependent energy difference of tens of millielectronvolts. Nonetheless, these PL peaks have also been explained by considering phonon-replicas [27].

In this Letter, we directly observe the discretized center-of-mass states of excitons from the lateral size dependence of experimental PL and optical absorption spectra of CdSe-NPLs. Both spectra are simultaneously interpreted and accurately modeled by considering the in-plane COM motion of excitons. In particular, quantum effects of spatial lateral confinement explain the size dependence of both the PL and absorption peak positions and widths. Our work provides an explanation of the hitherto open problem of understanding the effects of lateral size of NPLs on the properties of excitons. It can now be understood how variation of the lateral size of (quasi) two-dimensional materials provides a tool to continuously tune their optical properties, in addition to the discrete changes by adjustment of the thickness.

Four samples of CdSe-NPLs with a thickness of 4.5 monolayers ($L_z \simeq 1.4$ nm [4]) and different average lateral sizes were synthesized by following Ref. [13], see Supplemental Material Sec. I. The average lateral sizes ($L_x^{\text{avg}}, L_y^{\text{avg}}$) were determined from Transmission Electron Microscopy (TEM) images, as shown in Fig. 1(b), by assuming a Gaussian size distribution, see Fig. SM1 in the Supplemental Material. The results are shown in Table I, together with the NPL areas and aspect ratios $r_l \equiv L_x^{\text{avg}}/L_y^{\text{avg}}$. The samples are labeled based on their aspect ratio (first column in Table I). The data presented in this work are obtained from PL and optical absorption ensemble measurements on NPLs dispersed in hexane.

Fig. 1(c) shows the dependence of PL (dashed lines)

and absorption spectra (solid) on the NPL size. Spectra are normalized for comparison. Two clearly distinguishable absorption peaks are related to HH and LH exciton states. In agreement with Refs. [13, 16], by decreasing the aspect ratio, we observe: (i) a red shift of all features, (ii) decrease of the PL linewidth, (iii) decrease of the Stokes shift, and (iv) increase of the asymmetry (tail at the high-energy side) of the HH exciton peak. As mentioned above, the (iv)-th observation may be related to the presence of phonon replicas [27]. However, the latter cannot be dominant, since the small Stokes shifts in Fig. 1(c) imply weak exciton-phonon coupling. In addition, phonon replicas also give rise to a strong asymmetry at the low energy side of the PL peak, in contrast to the data in Fig. 1(c).

In order to interpret and explain the observations listed above, we now consider COM exciton states and their change with the lateral dimensions of the NPLs. Since the NPL thickness L_z is smaller than the bulk exciton Bohr radius, $a_B^{3D} = 5.4$ nm [16], excitons experience strong quantum confinement along the z -direction [14, 15, 28]. This strong confinement increases the exciton binding energy and reduces the Bohr radius to a quasi-2D value, $a_B^{2D} = 1.8$ -4.1 nm [4, 16, 29], which is smaller than the lateral sizes of the NPLs investigated in this work. Hence, excitons in a NPL are described by approximately factorizing their perpendicular and in-plane wave functions as [14, 15, 30]: $\Psi(z_e, z_h, \mathbf{r}, \mathbf{R}) \simeq u_{n_z}^e(z_e)u_{n_z}^h(z_h)\psi^{\text{rel}}(\mathbf{r})\psi_{n_x, n_y}^{\text{COM}}(\mathbf{R})$, where $z_{e,h}$ are the coordinates of electrons (e) and holes (h) perpendicular to the plane of the NPL, $\mathbf{r} = \mathbf{r}_e - \mathbf{r}_h$ and $\mathbf{R} = (m_e\mathbf{r}_e + m_h\mathbf{r}_h)/(m_e + m_h)$ are the relative and COM coordinates in the plane of the NPL, respectively, with m_e (m_h) being the electron (hole) effective mass, $m_e + m_h = M$ is the total exciton mass, while n_i are quantum numbers along the i -th direction. The wave functions $u_{n_z}^{e,h}$ give rise to a confinement energy of both the electron and the hole of $E_z = E_{n_z=1}^e(L_z) + E_{n_z=1}^h(L_z) = \pi^2\hbar^2/(2\mu L_z^2)$, where $\mu = m_e m_h/(m_e + m_h)$ is the reduced effective mass of

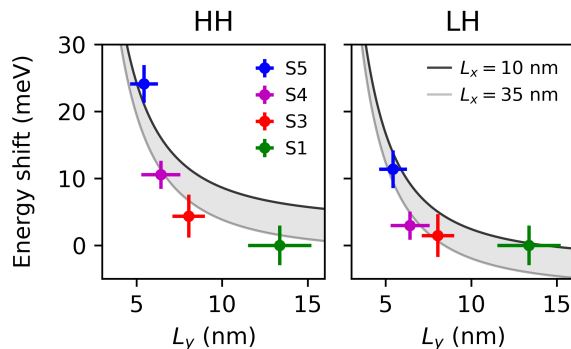


FIG. 2. Energy shift for HH (left) and LH (right) exciton absorption peaks from Fig. 1(c) as a function of the small lateral size L_y . This shift is considered with respect to the HH and LH energies of sample S1. Shaded areas are energy ranges obtained from Eq. (1) with L_x between 10 and 35 nm.

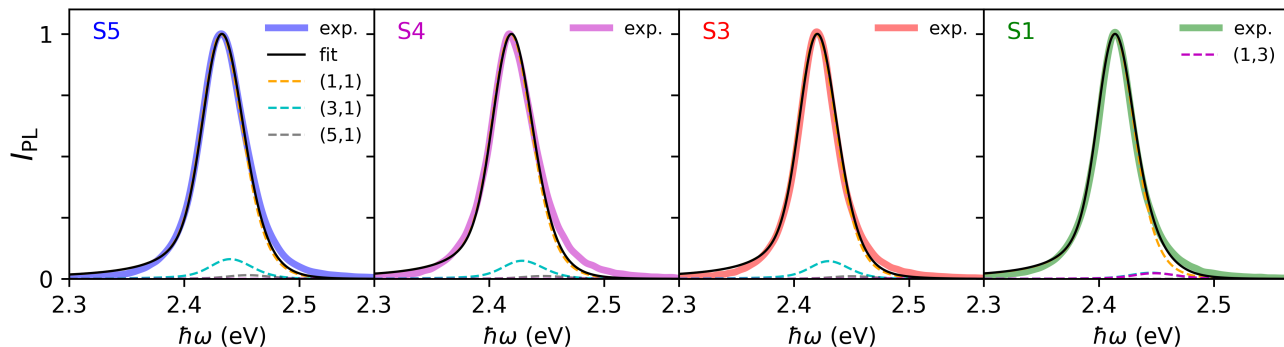


FIG. 3. Fits (black lines) of experimental photoluminescence spectra (coloured thick lines) from our CdSe-NPLs with different lateral sizes (see Table I). Our model considers the contribution of different exciton COM motional states (thin dashed coloured lines), with quantum numbers $\mathbf{n} = (n_x, n_y)$, whose energy and oscillator strength are influenced by the size distribution [Eq. (1) and (3)].

the e - h pair. The wave function $\psi^{\text{rel}}(\mathbf{r})$ describes the relative or internal exciton wave function, which can be obtained by using the appropriate Coulomb potential. The COM wave function $\psi_{n_x, n_y}^{\text{COM}}(\mathbf{R})$ is obtained by using the particle-in-a-box potential, resulting in COM exciton states with energy:

$$E_{n_x, n_y}(L_x, L_y) = \frac{\pi^2 \hbar^2}{2M} \left[\left(\frac{n_x}{L_x} \right)^2 + \left(\frac{n_y}{L_y} \right)^2 \right]. \quad (1)$$

For convenience, in what follows we use the notation $\mathbf{L} = (L_x, L_y)$ and $\mathbf{n} = (n_x, n_y)$, so that the dependence of the energy in Eq. (1) on the lateral size and quantum number is denoted as $E_{\mathbf{n}}(\mathbf{L})$.

The validity of our approach is first verified by focusing on the energy shift of the HH and LH absorption peaks, as the small lateral size (L_y) is varied, as shown in Fig. 2. This shift is considered from the exciton peak energies (for HH and LH) of the larger NPLs (sample S1, green dots). Vertical and horizontal bars depict the indetermination of the experimental peak energies and L_y , respectively. The shaded area represents the range of calculated energies from Eq. (1) with $\mathbf{n} = (1, 1)$, $m_e = 0.27 m_0$, the HH mass $m_{hh} = 0.45 m_0$, the LH mass $m_{lh} = 0.52 m_0$ [31], and L_x between 10 and 35 nm. The agreement between the calculated and experimental energy shift is a clear evidence of the role of spatial lateral confinement on the exciton COM motion.

According to the particle-in-a-box model, the COM wave function for the in-plane motion of an exciton is given by:

$$\psi_{n_x, n_y}^{\text{COM}}(x, y) = \sqrt{\frac{4}{L_x L_y}} \sin\left(\frac{n_x \pi x}{L_x}\right) \sin\left(\frac{n_y \pi y}{L_y}\right). \quad (2)$$

The oscillator strength for photoexcitation from the electronic ground state is non-zero only for odd values of both n_x and n_y , and is proportional to [30]:

$$f_{\mathbf{n}}(\mathbf{L}) = \left| \int_0^{L_x} \int_0^{L_y} dx dy \psi_{n_x, n_y}^{\text{COM}}(x, y) \right|^2 = \frac{4L_x L_y}{\pi^4 n_x^2 n_y^2}. \quad (3)$$

The oscillator strength described by Eq. (3) is in line with the experimental observation of an enhanced absorption cross section for larger NPLs [17]. Moreover, the inverse-square dependence on \mathbf{n} agrees with the observed asymmetry at the high energy side of the HH exciton absorption peak, as shown in Fig. 1(c).

To model PL and absorption spectra of an ensemble of NPLs, it is essential to average over the known population distribution $D(\mathbf{L})$ of CdSe-NPLs in the sample, which is a Gaussian distribution reported in Fig. SM1 of the Supplemental Material. PL spectra are due to photon emission from HH excitons in COM motional states with quantum numbers $\mathbf{n} = (n_x, n_y)$. This leads to the following expression for the PL intensity at photon energy $\hbar\omega$:

$$I_{\text{PL}}(\hbar\omega) = \sum_{\mathbf{n}} \int d\mathbf{L} D(\mathbf{L}) f_{\mathbf{n}}(\mathbf{L}) e^{-\hbar\omega/k_B T} \cdot \mathcal{V}(\hbar\omega - E^{\text{HH}} - E_{\mathbf{n}}^{\text{HH}}(\mathbf{L}); \Gamma^{\text{HH}}(\hbar\omega), \sigma^{\text{HH}}). \quad (4)$$

The exponential factor is due to the classical Maxwell-Boltzmann (MB) distribution over thermalized COM motional states. The broadening of each of these states is modelled by the Voigt distribution [23, 25], $\mathcal{V}(\hbar\omega - E_0; \Gamma^{\text{HH}}(\hbar\omega), \sigma^{\text{HH}})$, centered at $E_0 = E^{\text{HH}} + E_{\mathbf{n}}^{\text{HH}}(\mathbf{L})$, where E^{HH} is the exciton state with zero COM energy, which is determined also by the z -confinement and Stokes shift. The term $E_{\mathbf{n}}^{\text{HH}}(\mathbf{L})$ is calculated from Eq. (1). Γ^{HH} and σ^{HH} are the linewidths of the Lorentzian and Gaussian distribution defining \mathcal{V} , respectively. The former accounts for the exciton-phonon interaction which, according to the Urbach rule [32], is given by: $\Gamma^{\text{HH}}(\hbar\omega) = \Gamma_0^{\text{HH}} / (e^{[E^{\text{HH}} + E_{\mathbf{n}}^{\text{HH}}(\mathbf{L}) - \hbar\omega]/k_B T} + 1)$. σ^{HH} is here attributed to the inhomogeneous broadening due to structural, size-independent disorder; e.g. non-flatness of NPLs, effects of surface ligands on the NPLs, or to the deviation of the shape of the NPLs from perfect rectangles. The only fit parameters for modeling PL spectra from Eq. (4) for all samples are E^{HH} , Γ_0^{HH} , and σ^{HH} .

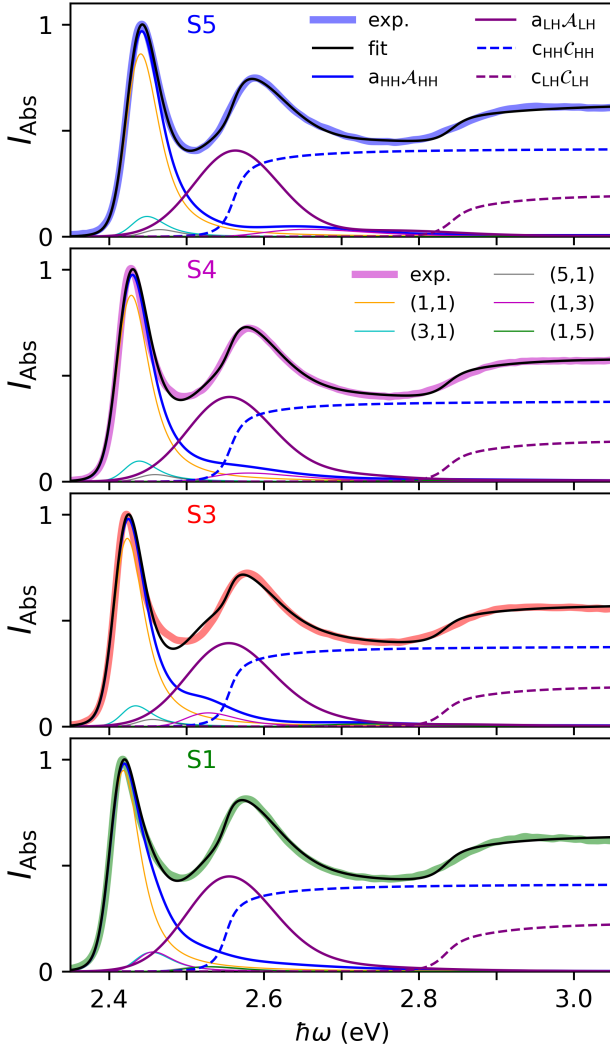


FIG. 4. Fits (black lines) of our model given by Eqs. (5), (6) and (7) to the experimental absorption spectra. The presence of exciton COM motional states, $\mathbf{n} = (n_x, n_y)$ (depicted by coloured thin lines), and their dependence on the lateral sizes of the NPLs, explains and reproduces the change in the asymmetry at the high-energy side of the HH absorption peak.

Fig. 3 shows the obtained PL fits (black thin lines) which agree very well with the experimental spectra (thick colored lines) for every sample. The fits are obtained with $\Gamma_0^{\text{HH}} = 26 \pm 1$ meV and $\sigma^{\text{HH}} = 14 \pm 1$ meV for all samples. The contribution of different states is also depicted (thin lines). For rectangular NPLs ($r_l > 1$), besides the main PL from (1,1) states, the contribution at higher energies is due to (3,1) (magenta) and (5,1) (grey) states. The small contribution from the (5,1) states is due to the decrease of the oscillator strength with \mathbf{n} , see Eq. (3), as well as to the MB distribution. Due to the square shape of the NPLs in the S1 sample ($r_l = 1$), the (3,1) and (1,3) (cyan) states contribute with a similar oscillator strength and energy. Since Γ_0^{HH} and σ^{HH} are the same for all samples, the decreasing

experimental PL linewidth, by going from sample S5 to sample S1, is explained by a reduction of the effects of the lateral size distribution of the NPLs via $D(\mathbf{L})$ and, in turn $f_{\mathbf{n}}(\mathbf{L})$.

The exciton absorption is modeled similarly to the PL and is given by:

$$\mathcal{A}^J(\hbar\omega) = \sum_{\mathbf{n}} \int d\mathbf{L} D(\mathbf{L}) f_{\mathbf{n}}(\mathbf{L}) \cdot \mathcal{V}(\hbar\omega - E^J - E_{\mathbf{n}}^J(\mathbf{L}); \Gamma^J(\hbar\omega), \sigma^J), \quad (5)$$

where $J = \text{HH, LH}$. Note, that the MB distribution does not appear in Eq. (5), since the initial state for absorption is the electronic ground state of a NPL. Transitions from the valence to the conduction band (continuum) need also to be taken into account and are calculated as:

$$\mathcal{C}^J(\hbar\omega) = \sum_{\mathbf{n}} \int d\mathbf{L} D(\mathbf{L}) f_{\mathbf{n}}(\mathbf{L}) \cdot \int_{-\infty}^{\infty} d\epsilon_0 \mathcal{V}(\hbar\omega - \epsilon_0; \Gamma_c^J(\hbar\omega), \sigma_c^J) \cdot \Theta(\epsilon_0 - E_X^J - E^J - E_{\mathbf{n}}^J(\mathbf{L})), \quad (6)$$

where Γ_c^J and σ_c^J are the Lorentzian and Gaussian linewidths of the continuum, respectively, $\Theta(x)$ is the step-function (that is, $\Theta(x) = 1$ for $x > 0$ and zero otherwise), and E_X^J is the exciton binding energy, which is defined to be positive. By means of Eqs. (5) and (6), the absorption due to all above-mentioned states is:

$$I_{\text{Abs}}(\hbar\omega) = a^{\text{HH}} \mathcal{A}^{\text{HH}}(\hbar\omega) + a^{\text{LH}} \mathcal{A}^{\text{LH}}(\hbar\omega) + c^{\text{HH}} \mathcal{C}^{\text{HH}}(\hbar\omega) + c^{\text{LH}} \mathcal{C}^{\text{LH}}(\hbar\omega), \quad (7)$$

where each contribution is weighted with fitted coefficients a^J and c^J that take into account the optical dipole moments involving the relative motion of electrons and holes in the exciton and continuum states, respectively. The values of E^{HH} , Γ_0^{HH} , and σ^{HH} obtained by fits to the PL spectra are also used to calculate the contribution from $\mathcal{A}^{\text{HH}}(\hbar\omega)$. For LH excitons, E^{LH} , Γ_0^{LH} , and σ^{LH} are obtained from fits to the absorption spectra. The parameters Γ_c^J , and E_X^J are also fitted, while σ_c^J is taken to be zero for simplicity, as we expect delocalized continuum states to be less affected by local disorder.

Fig. 4 shows the obtained fits (black thin lines) and the experimental absorption (colored thick lines). The total contribution from HH (blue solid lines) and LH excitons (magenta solid lines) are also shown together with the corresponding continuum contributions (dashed lines). Thin colored lines depict different \mathbf{n} -states for HH excitons. Our model thus reproduces very well the entire absorption spectra for different lateral sizes of NPLs. The fitting procedure results in exciton binding energies equal to $E_X^{\text{HH}} = 135 \pm 2$ meV and $E_X^{\text{LH}} = 301 \pm 4$ meV, which are independent of the lateral sizes to within the uncertainty. This is to be expected,

since $L_x, L_y > a_B^{2D}$ for all samples, and consistent with our separable ansatz for the exciton wave functions on which our model is based. Other fitting parameters are listed in Table SMI of the Supplemental Material. Note that all fit parameters do not depend on the lateral sizes of the NPLs, as expected. The asymmetry of the HH peak clearly depends on the presence of different exciton COM motional states. The (1,3) state redshifts on going from sample S5 to sample S1 due to the increase of the lateral size L_y . In addition, the enhanced HH asymmetry for the S1 sample results from the similar contribution of (1,3) and (3,1) states.

In conclusion, we demonstrated that effects of the lateral size of CdSe NPLs on PL and optical absorption spectra can be fully attributed to the quantized exciton COM motion. The experimental spectra can be reproduced theoretically on the basis of the simple particle-in-a-box model for the translational motion of the exciton within a NPL. Importantly, it was not

necessary to take into account size-dependent effects of phonons on PL and absorption spectra. Our results show that variation of the lateral size of (quasi) two-dimensional materials provides a tool to tune their excitonic and therefore optoelectronic properties in addition to modifying the thickness. The new insights also open the road to studying nontrivial quantum effects such as the Berry phase on the COM motion of topological excitons in NPLs consisting of topological insulator materials.

ACKNOWLEDGMENTS

L. D. A. S. and M. F. thank A. W. Achtstein for the very helpful discussions. This work is part of the research program TOP-grants with project number 715.016.002, which is financed by the Netherlands Organization for Scientific Research (NWO).

-
- [1] S. Ithurria and B. Dubertret, Quasi 2D colloidal CdSe platelets with thicknesses controlled at the atomic level, *J. Am. Chem. Soc.* **130**, 16504 (2008).
- [2] J. Yu and R. Chen, Optical properties and applications of twodimensional CdSe nanoplatelets, *InfoMat*, **1** (2020).
- [3] A. Naeem, F. Masia, S. Christodoulou, I. Moreels, P. Borri, and W. Langbein, Giant exciton oscillator strength and radiatively limited dephasing in two-dimensional platelets, *Phys. Rev. B* **91**, 121302(R) (2015).
- [4] A. W. Achtstein, A. Schliwa, A. Prudnikau, M. Hardzei, M. V. Artemyev, C. Thomsen, and U. Woggon, Electronic structure and excitonphonon interaction in two-dimensional colloidal CdSe nanosheets, *Nano Lett.* **12**, 3151 (2012).
- [5] R. Tomar, A. Kulkarni, K. Chen, S. Singh, D. van Thourhout, J. M. Hodgkiss, L. D. A. Siebbeles, Z. Hens, and P. Geiregat, Charge carrier cooling bottleneck opens up nonexcitonic gain mechanisms in colloidal CdSe quantum wells, *J. Phys. Chem. C* **123**, 9640 (2019).
- [6] A. W. Achtstein, O. Marquardt, R. Scott, M. Ibrahim, T. Riedl, A. V. Prudnikau, A. Antanovich, N. Owschimikow, J. K. N. Lindner, M. Artemyev, and U. Woggon, Impact of shell growth on recombination dynamics and excitonphonon interaction in CdSeCdS coreshell nanoplatelets, *ACS Nano* **12**, 9476 (2018).
- [7] M. Li, M. Zhi, H. Zhu, W.-Y. Wu, Q.-H. Xu, M. H. Jhon, and Y. Chan, Ultralow-threshold multiphoton-pumped lasing from colloidal nanoplatelets in solution, *Nat. Commun.* **6**, 8513 EP (2015).
- [8] R. Scott, A. W. Achtstein, A. Prudnikau, A. Antanovich, S. Christodoulou, I. Moreels, M. Artemyev, and U. Woggon, Two photon absorption in IIVI semiconductors: The influence of dimensionality and size, *Nano Lett.* **15**, 4985 (2015).
- [9] J. Heckmann, R. Scott, A. V. Prudnikau, A. Antanovich, N. Owschimikow, M. Artemyev, J. I. Climente, U. Woggon, N. B. Grosse, and A. W. Achtstein, Directed two-photon absorption in CdSe nanoplatelets revealed by k -space spectroscopy, *Nano Lett.* **17**, 6321 (2017).
- [10] J. Q. Grim, S. Christodoulou, F. Di Stasio, R. Krahn, R. Cingolani, L. Manna, and I. Moreels, Continuous-wave biexciton lasing at room temperature using solution-processed quantum wells, *Nat. Nanotechnol.* **9**, 891 EP (2014).
- [11] Z. Yang, M. Pelton, I. Fedin, D. V. Talapin, and E. Waks, A room temperature continuous-wave nanolaser using colloidal quantum wells, *Nat. Commun.* **8**, 143 (2017).
- [12] S. Ithurria, M. D. Tessier, B. Mahler, R. P. S. M. Lobo, B. Dubertret, and A. L. Efros, Colloidal nanoplatelets with two-dimensional electronic structure, *Nat. Mater.* **10**, 936 (2011).
- [13] G. H. V. Bertrand, A. Polovitsyn, S. Christodoulou, A. H. Khan, and I. Moreels, Shape control of zincblende CdSe nanoplatelets, *Chem. Commun.* **52**, 11975 (2016).
- [14] F. Rajadell, J. I. Climente, and J. Planelles, Excitons in core-only, core-shell and core-crown CdSe nanoplatelets: Interplay between in-plane electron-hole correlation, spatial confinement, and dielectric confinement, *Phys. Rev. B* **96**, 035307 (2017).
- [15] M. Richter, Nanoplatelets as material system between strong confinement and weak confinement, *Phys. Rev. Materials* **1**, 016001 (2017).
- [16] S. Ithurria, G. Bousquet, and B. Dubertret, Continuous transition from 3D to 1D confinement observed during the formation of CdSe nanoplatelets, *J. Am. Chem. Soc.* **133**, 3070 (2011).
- [17] A. Yeltik, S. Delikanli, M. Olutas, Y. Kelestemur, B. Guzelturk, and H. V. Demir, Experimental determination of the absorption cross-section and molar extinction coefficient of colloidal CdSe nanoplatelets, *J. Phys. Chem. C* **119**, 26768 (2015).
- [18] C. She, I. Fedin, D. S. Dolzhenkov, P. D. Dahlberg, G. S. Engel, R. D. Schaller, and D. V. Talapin, Red, yellow, green, and blue amplified spontaneous emission and las-

- ing using colloidal CdSe nanoplatelets, *ACS Nano* **9**, 9475 (2015).
- [19] M. Olutas, B. Guzelturk, Y. Kelestemur, A. Yeltik, S. Delikanli, and H. V. Demir, Lateral size-dependent spontaneous and stimulated emission properties in colloidal CdSe nanoplatelets, *ACS Nano* **9**, 5041 (2015).
- [20] Q. Li and T. Lian, Area- and thickness-dependent biexciton Auger recombination in colloidal CdSe nanoplatelets: Breaking the “universal volume scaling law”, *Nano Lett.* **17**, 3152 (2017).
- [21] Q. Li and T. Lian, A model for optical gain in colloidal nanoplatelets, *Chem. Sci.* **9**, 728 (2018).
- [22] R. F. Schnabel, R. Zimmermann, D. Bimberg, H. Nickel, R. Lösch, and W. Schlapp, Influence of exciton localization on recombination line shapes: InIn_xGa_{1-x}As/GaAs quantum wells as a model, *Phys. Rev. B* **46**, 9873 (1992).
- [23] A. W. Achtstein, R. Scott, S. Kickhöfel, S. T. Jagsch, S. Christodoulou, G. H. V. Bertrand, A. V. Prudnikau, A. Antanovich, M. Artemyev, I. Moreels, A. Schliwa, and U. Woggon, *p*-state luminescence in CdSe nanoplatelets: Role of lateral confinement and a longitudinal optical phonon bottleneck, *Phys. Rev. Lett.* **116**, 116802 (2016).
- [24] D. P. Morgan, C. J. A. Maddux, and D. F. Kelley, Transient absorption spectroscopy of CdSe nanoplatelets, *J. Phys. Chem. C* **122**, 23772 (2018).
- [25] R. Scott, A. V. Prudnikau, A. Antanovich, S. Christodoulou, T. Riedl, G. H. V. Bertrand, N. Owschimikow, J. K. N. Lindner, Z. Hens, I. Moreels, M. Artemyev, U. Woggon, and A. W. Achtstein, A comparative study demonstrates strong size tunability of carrier-phonon coupling in CdSe-based 2D and 0D nanocrystals, *Nanoscale* **11**, 3958 (2019).
- [26] J. F. Specht, R. Scott, M. Corona Castro, S. Christodoulou, G. H. V. Bertrand, A. V. Prudnikau, A. Antanovich, L. D. A. Siebbeles, N. Owschimikow, I. Moreels, M. Artemyev, U. Woggon, A. W. Achtstein, and M. Richter, Size-dependent exciton substructure in CdSe nanoplatelets and its relation to photoluminescence dynamics, *Nanoscale* **11**, 12230 (2019).
- [27] M. D. Tessier, L. Biadala, C. Bouet, S. Ithurria, B. Abecassis, and B. Dubertret, Phonon line emission revealed by self-assembly of colloidal nanoplatelets, *ACS Nano* **7**, 3332 (2013).
- [28] F. G. Flórez, L. D. A. Siebbeles, and H. T. C. Stoof, Effects of two-dimensional material thickness and surrounding dielectric medium on coulomb interactions and excitons, arXiv:2002.05921 [cond-mat] (2020), arXiv:2002.05921 [cond-mat].
- [29] M. D. Tessier, C. Javaux, I. Maksimovic, V. Lorient, and B. Dubertret, Spectroscopy of single CdSe nanoplatelets, *ACS Nano* **6**, 6751 (2012).
- [30] R. Zimmermann and E. Runge, Excitons in narrow quantum wells: Disorder localization and luminescence kinetics, *physica status solidi (a)* **164**, 511 (1997).
- [31] R. Benchamekh, N. A. Gippius, J. Even, M. O. Nestoklon, J.-M. Jancu, S. Ithurria, B. Dubertret, A. L. Efros, and P. Voisin, Tight-binding calculations of image-charge effects in colloidal nanoscale platelets of CdSe, *Phys. Rev. B* **89**, 035307 (2014).
- [32] H. Haug and S. W. Koch, *Quantum Theory of the Optical and Electronic Properties of Semiconductors*, 5th ed. (WORLD SCIENTIFIC, 2009).